論文 / 著書情報
Article / Book Information

Title	Mixed mode fracture toughness of adhesively bonded joints with residual stress
Authors	Kazumasa Shimamoto, Yu Sekiguchi, Chiaki Sato
Citation	International Journal of Solids and Structures, Volume 102-103, pp. 120-126
Pub. date	2016, 12
DOI	http://dx.doi.org/10.1016/j.ijsolstr.2016.10.011
Creative Commons	See next page.
Note	This file is author (final) version.

License

Mixed mode fracture toughness of adhesively bonded joints with residual stress

Kazumasa Shimamoto [a], Yu Sekiguchi [b,*], Chiaki Sato [b]

[a] Department of Mechano-Micro Engineering, Interdisciplinary Graduate School of Science and Engineering, Tokyo Institute of Technology, 4259 Nagatsuta-cho, Midori-ku, Yokohama 226-8503, Japan

[b] Institute of Innovative Research (IIR), Tokyo Institute of Technology, 4259 Nagatsuta-cho, Midori-ku, Yokohama 226-8503, Japan

[*] Corresponding author. Tel/Fax: +81 45 924 5012; E-mail address: sekiguchi.y.aa@m.titech.ac.jp (Y. Sekiguchi).

Abstract

Adhesively bonded double cantilever beam (DCB) test specimens with residual stress were manufactured. Deforming the adherends during the curing process caused the DCB specimens to curve due to the residual stress and shear load arose at the adhesive layer. Therefore, mixed mode fractures were generated by applying mode I loading to the specimens. The relation between the specimen curvature and the strain energy due to the residual stress was theoretically investigated and the mode II energy release rate for each specimen was calculated using measured specimen curvature. Because the mode I energy release rate for each specimen can be calculated with the DCB test result, the fracture toughness in mixed mode conditions was discussed. By manufacturing the specimens with different residual stresses, mixed mode fracture tests with various mixed mode ratios were conducted and the effect of the mixed mode ratio on the energy release rates was investigated.

Keywords: Adhesive joints; Energy release rate; Mixed mode fracture; Residual stress

1. Introduction

Adhesive bonding has recently been used as a structural joining method for vehicles, aircrafts, ships, and so on. The fracture toughness and durability of adhesively bonded joints are essential in industrial uses and evaluation methods, such as for energy release rate, joint strength and creep resistance, have been widely discussed. Fracture modes, for instance mode I, mode II and mixed mode I/II, as shown in Fig. 1, change the energy release rate of the adhesively bonded joints. Therefore, methods to evaluate facture toughness have been derived for each mode. In the case of mode I fractures, double cantilever beam (DCB) and tapered-DCB tests have been standardized (ASTM D3433-99, 2012; ASTM D5528-01, 2007; ISO 15024, 2001). For mode II fractures, end notched flexure (ENF) (ASTM D7905-14, 2014; Banea et al., 2012; Chaves et al., 2014a; da Silva et al., 2010, 2012; Davies et al., 1999), four point ENF (4ENF) (Chaves et al., 2014a; da Silva et al., 2010; Davies et al., 1999; Martin and Davidson, 1999; Schuecker and Davidson, 2000) and end loaded split (ELS) tests (Blackman et al., 2005; Chaves et al., 2014a; da Silva et al., 2010, 2012; Davies et al., 1999) have been devised using DCB specimens. In addition, using DCB specimens, dual actuator loading (DAL) (Chaves et al., 2011, 2014a, 2014b; Dillard et al., 2006; Singh et al., 2010), mixed mode bending (MMB) (ASTM D6671-06, 2006; Chaves et al., 2014a; Oliveira et al., 2007; Reeder and Rews Jr., 1990), and spelt loading jig (SPELT) tests (Fernlund and Spelt, 1994) have been devised for mixed mode fractures. These mixed mode test methods require the original loading jigs or original test machines to apply mixed mode loads, but a wide range of mixed mode ratios spanning mode I and mode II can be tested. Using the original specimens, asymmetric double cantilever beam (ADCB) (Xiao et al., 1993), single leg bending (SLB) (Davidson and Sundararaman, 1996; Yoon and Hong, 1990) and asymmetric tapered-DCB (ATDCB) tests (Park and Dillard, 2007) have also been devised for mixed mode fracture cases. Although only the opening load with a standard tensile testing machine is required for the ADCB and ATDCB tests, the mixed mode ratio is limited.

In many practical situations of joint failures, mixed mode fracture is dominant because the stress distribution at the joints is very complicated. Therefore, it is important to obtain energy release rates

with a wide range of mixed mode ratios. One source of combined loads is the residual thermal stress at the joints. When different materials are jointed together, their different thermal expansion/contraction characteristics generate residual stress (Franco and Royer-Crafagni, 2016; Nairn, 2000; Shimamoto et al., 2016). Because the difference between the curing temperature and room temperature cannot be avoided with heat cure adhesives, residual thermal stress arises during the curing process. Residual stress is also generated when the adhesive is cured while the adherend is deformed such as bent lamination, which is well known for laminated glass or glue-laminated-timber (Galuppi and Royer-Carfagni, 2015a). With such cases, residual bending stress arises at the adherend and can be another factor of the mixed mode fractures.

In this paper, the manufacturing process of a DCB test specimen with a residual stress (DCB-rs) is investigated. The adherends are elastically deformed by an external load during the curing process. Shear stress arises at the adhesive layer when the load is removed. The residual stress was calculated by measuring the curvature of the DCB-rs specimens. The applied opening load caused mixed mode fracturing of the DCB-rs specimens. The residual stress can be arbitrarily changed by controlling the magnitude of the adherends' deformation during the curing process. Therefore, a wide range of mixed mode ratios can be tested with the DCB-rs specimens.

2. Description of a double cantilever beam specimen with residual stress

2.1 Manufacturing process of the DCB-rs specimens

The 4ENF test is a pure mode II fracture tests that is used to generate shear loads at the adhesive layer, as shown in Fig. 2 (a)-(c). Conversely, when the specimen is kept bent during the curing process, as shown in Fig. 2 (d)-(g), the specimen remains curved even after the external load is released. Hence, shear stress is generated at the adhesive layer. Specimens with different residual stress can be manufactured by changing the magnitude of the bend.

A four point bending jig, as shown in Fig. 3, was used to manufacture the DCB-rs specimens. The adherends were set to the jig after adhesive was applied and they were sandwiched together. They were

then put into an electric furnace for curing. Then, the specimen was taken off of the jig. Because pure mode II loading was only generated between the inner load points of the four point bending jig, adhesive was pasted inside the inner load points.

2.2 Stress distribution of the adherends

The radius of curvature of a couple of beams bonded together has been derived in the case of bi-metal thermostats (Timoshenko 1925), where the bending moment is generated by the gap of the coefficient of expansion. In this study, a constant moment is applied to the adherends by fixing the specimen to the four-point bending jig. Using the same derivative method as Timoshenko (1925), the relation between the stress and the radius of curvature is investigated for the DCB-rs specimens in the assumption of Euler-Bernoulli beam theory. Thus, the radius of curvature of the adherends is constant, denoted as ρ'. The stress of each adherend before the release from the jig is given by

$$\sigma_{\text{before}} = -E\frac{\left(y-\frac{t+t_{\text{a}}}{2}\right)}{\rho'} \tag{1}$$

for the upper adherend and

$$\sigma_{\text{before}} = -E\frac{\left(y+\frac{t+t_{\text{a}}}{2}\right)}{\rho'} \tag{2}$$

for the lower adherend, where E is the Young's modulus of the adherend, y is the distance from the center of the adhesive layer, t is the thickness of the adherend, and t_{a} is the thickness of the adhesive layer. Conversely, the stress at the adhesive layer is zero because the adhesive is not cured and still liquid-like when the specimen is bent. When the specimen is released from the jig after the cure, the radius of the specimen curvature increased and the stress of the adherends due to the bending is changed to

$$\sigma_{\text{bend}} = -E\frac{\left(y-\frac{t+t_{\text{a}}}{2}\right)}{\rho} \tag{3}$$

for the upper adherend and

$$\sigma_{\text{bend}} = -E\frac{\left(y+\frac{t+t_{\text{a}}}{2}\right)}{\rho} \tag{4}$$

for the lower adherend, where ρ is the radius of the specimen curvature after the release. After the adhesive is cured, the adhesive layer inhibits the change of the strain at the interface and a stress arises in the longitudinal direction of the adherends. To constrain the interface, the upper adherend stress acts in tension and the lower one acts in compression with constant values. Denoting the magnitude of this stress as $\sigma_{\text{constraint}}$, the stress acting to the adherends after the release is expressed as

$$\sigma_{\text{after}} = \sigma_{\text{bend}} + \sigma_{\text{constraint}} \tag{5}$$

for the upper adherend and

$$\sigma_{\text{after}} = \sigma_{\text{bend}} - \sigma_{\text{constraint}} \tag{6}$$

for the lower adherend. Because no external force acts at the specimen after being manufactured, the moment acting on the specimen is zero, i.e.,

$$M = \int_S \sigma_{\text{after}} y dS = 0, \tag{7}$$

where S is a cross sectional area of the specimen. Then, the stress due to the constraint is obtained as

$$\sigma_{\text{constraint}} = \frac{Et^2}{6\rho(t+t_{\text{a}})}, \tag{8}$$

where the moment at the adhesive layer is assumed to be small enough to be neglected. In addition, the stress after the release is obtained as

$$\sigma_{\text{after}} = \left(\frac{4t^2+6tt_{\text{a}}+3t_{\text{a}}^2}{6(t+t_{\text{a}})} - y\right)\frac{E}{\rho} \tag{9}$$

for the upper adherend and

$$\sigma_{\text{after}} = -\left(\frac{4t^2+6tt_{\text{a}}+3t_{\text{a}}^2}{6(t+t_{\text{a}})} + y\right)\frac{E}{\rho} \tag{10}$$

for the lower adherend.

2.3 Calculation of the energy release rate

In the DCB test with the DCB-rs specimens, tensile load P is applied to the end of the specimen to propagate the crack. The tensile load contributes to opening mode, and the residual stress at the adhered part contributes to sliding mode. Therefore, the mode I and mode II energy release rates can be

calculated separately. Using the experimental compliance method (ECM), the mode I energy release rate is obtained as

$$G_{\mathrm{I}} = \frac{nP\delta}{2ba}\ \frac{F}{N}, \tag{11}$$

where δ is the total beam opening displacement, a is the crack length, b is the specimen width, n is the constant determined by the slope of the plot of log C versus log a, as shown in Fig. 4, C is the compliance, which is given by $C = \delta / P$, and F and N are correction factors of large displacement and end-blocks, respectively (Blackman et al., 2003, Sekiguchi et al., 2016). The correction for large displacements is given by

$$F = 1 - \frac{3}{10}\left(\frac{\delta}{a}\right)^2 - \frac{3}{2}\left(\frac{l_1\delta}{a^2}\right), \tag{12}$$

where l_1 is the distance between the center of the adherend and the center of the piano hinge pin in the thickness direction. Because the load is applied to the DCB-rs specimen via piano hinges, the correction of the end-block is given by N=1.

Conversely, simple beam theory is applied in the analysis of the mode II energy release rate. In the case of the 4ENF tests, it has been identified that the beam theory method shows the identical trend in comparison with the finite element analysis (FEA) (Martin and Davidson, 1999). Because same deformation as the 4ENF tests is applied to the DCB-rs specimens, it can be indicated that the beam theory calculation for the mode II is reasonably accurate. The strain energy of the adherends due to the residual stress is given as

$$U_{\mathrm{r}} = \int_V \frac{\sigma\varepsilon}{2} dV, \tag{13}$$

where σ, ε, and V are the stress, strain, and volume of the specimen, respectively. Substituting Eqs. (9) and (10) into Eq. (13), leads to

$$U_{\mathrm{r}} = \frac{Et^3}{9\rho^2}\left(1 + \frac{t_{\mathrm{a}}}{t}\right) b(a_1 - a), \tag{14}$$

where a_1 is the length from the loading point to the farther end of the adhesive layer, as shown in Fig. 5. The elastic energy of the adhesive layer and the second order and higher order terms of t_{a}/t are

neglected. When the crack propagates by opening mode loading, the energy due to the residual stress stored at the adhered part of the specimen is released. Therefore, the energy release rate due to the residual stress is given by

$$G_{\mathrm{r}} = -\frac{1}{b}\frac{dU_{\mathrm{r}}}{da} = \frac{Et^3}{9\rho^2}\left(1+\frac{t_{\mathrm{a}}}{t}\right). \tag{15}$$

Because there is no other mode II loading, the mode II energy release rate is given as

$$G_{\mathrm{II}} = G_{\mathrm{r}} = \frac{Et^3}{9\rho^2}\left(1+\frac{t_{\mathrm{a}}}{t}\right). \tag{16}$$

The mixed mode angle, ψ, is denoted as

$$\psi = \tan^{-1}\sqrt{\frac{G_{\mathrm{II}}}{G_{\mathrm{I}}}}, \tag{17}$$

where ψ=0° refers to pure mode I and ψ=90° refers to pure mode II loading conditions.

3 Experimental

3.1 Materials and specimens

The configuration and dimensions of the specimens are shown in Fig. 5. Spring steel (SUP10) was selected for the adherends because over estimation of the energy release rate due to the plastic deformation of the adherends can be avoided by using materials with a wide elastic region. The material properties of the adherend are shown in Table 1. The adherends were bonded with a two component epoxy adhesive (denatite 2204, Nagase ChemteX Corporation, Osaka, Japan). The adhesive was cured at 100 °C for 30 min. The bonding span was set to 56 mm to obtain symmetrical residual deformation. The initial crack length was set to 50 mm. Polytetrafluoroethylene (PTFE) sheets with a 0.1-mm thickness were inserted between the adherends at both ends to create the initial crack and control the thickness of the adhesive layer. In addition, glass beads with a diameter 100 μm were added to the adhesive layer to control the thickness more accurately. The bonding surfaces of the adherends were sandblasted with #120 alumina grit (SG-118-120, Hozan Tool Industrial Co. Ltd., Osaka, Japan) at an air pressure of 0.7 MPa. Two piano hinges were attached at the edge of each adherend for the DCB test.

3.2 Specimen manufacturing

The four-point bending jig is shown in Fig. 3 (a). This jig consists of a lower base, upper base, spacers and nuts. The indentation depth, *d*, as shown in Fig. 3(b), is controlled by the length of the spacers. The jig has an inner span of 100 mm and outer span of 150 mm. The curvature of each specimen was measured with a laser displacement sensor (LK-H022K, KEYENCE Co., Osaka, Japan) while moving the specimens with the x-y motorized stages under the sensor. The radius of the curvature was calculated with a least squares method within the adhesively bonded area.

3.3 Double cantilever beam test

Mode I fracture tests were conducted using the DCB-rs specimens at a crosshead speed of 2 mm/min. The load was measured with tension/compression load cells placed at both crossheads, the fracture process was recorded by a CCD monochrome camera, and the crack length was measured from the recorded pictures afterward. The load, displacement and crack lengths during crack propagation was used to calculate the critical energy release rate. In addition, standard ENF test specimens using the same adherends were manufactured, and a mode II fracture test following ASTM D7905-14 (2014) was conducted. Then, the G_{II} was calculated using the compliance based beam method (CBBM) (de Moura et al., 2009).

4 Results and discussion

4.1 Mode I energy release rates

The load versus displacement results of the DCB tests with the DCB-rs specimens are shown in Fig. 6. When the residual effect on the specimen was small, the load decreased with increasing displacements after reaching the initial peak, as shown in Fig. 6 (a). This is similar to standard DCB test results. However, the region after the initial peak can be divided into two regions by increasing the residual effect, as shown in Fig. 6 (b). First, the load decreased with increasing displacements. Then,

the load increased again. When the residual effect increased further, the first region disappeared and the load sharply dropped after reaching the initial peak with rapid crack propagation. Then, the load re-increasing region started, as shown in Fig. 6 (c). The mode I critical energy release rate is shown in Fig. 7. The value was almost constant when the crack started propagating. After the crack propagated more than half the length of the adhesive layer, the value increased to the pure mode I value. Figure 8 shows the crack length and load change against the displacement. The load re-increasing region appeared when approximately 70 to 80 % of the adhered part was fractured. The crack continuously propagated in the load decreasing region, but it merely propagated in the load re-increasing region. Therefore, it is indicated that the fracture condition changed between the regions. When the adhered length becomes shorter, the adhesive layer cannot hold the residual deformation and the residual stress is released. Then, the radius of specimen curvature increases. Because the mode II fracture energy release rate is in inversely proportional to the square of the radius of specimen curvature, the increase of the radius of specimen curvature represents the decrease of mode II contribution to the mixed mode ratio. Therefore, the fracture shifted to the pure mode I condition in the load re-increasing region. Conversely, the mode I value in the load decreasing region was almost constant, i.e. the mixed mode ratio in this region is thought to be constant. Hence, the mode I value in the load decreasing region was used for the discussion of the mixed mode effect.

4.2 Mode II energy release rate

The measured deformations of the specimens with indentation depths of d =1.0, 3.0, and 5.0 mm are shown in Fig. 9 (a). The residual deformations increased with longer indentation depths. The relation between the indentation depth and radius of the specimen curvature before the release is obtained as

$$d = \frac{(l_{\mathrm{out}}-l_{\mathrm{in}})(l_{\mathrm{out}}+2l_{\mathrm{in}})}{12\rho'}, \tag{18}$$

using simple beam theory, where l_{in} and l_{out} are the inside and outside spans of the four point bending jig, respectively. In addition, the relation between the radiuses before and after the release is obtained

as $\rho'/\rho = 3/4$ when neglecting the adhesive layer thickness. Therefore, the indentation depth can be back-calculated from the measured radius of the specimen curvature. The results for each specimen are listed in Table 2. It was clarified that the indentation depth was slightly deeper than the target depth. Additionally, the G_{II} increased with increasing indentation depths. In the case with an indentation depth of 6 mm, the specimen broke when it was released from the jig. The G_r calculated in the case for d=6 mm was 1744 J/m^2. Conversely, the G_{II} with the ENF test was slightly over 1600 J/m^2. This indicates that the specimen was fractured by the residual stress.

Figure 9 (b) shows the deformation of the adhered area with circular fitting curves. The curvature is theoretically constant at the bonded area because a constant moment was applied using the four-point bending jig. It is confirmed that the circular fitting, i.e., constant radius of specimen curvature, is suitable for the proposed manufacturing procedure. However, it has been reported that the deformed shape largely affects the stress distribution at the boundary of the adhesive layer (Galuppi and Royer-Carfagni, 2015b, 2015c) in the case of the bent lamination. The stress distribution can be easily changed by varying the manufacturing process. Therefore, it would be preferred to carefully check the specimen curvature after each manufacturing.

4.3 Mixed-mode energy release rates

The experimental results of the relation between the mode I and mode II energy release rates is shown in Fig. 10. The closed circles are the results from specimens 1 to 8 in Table 2. Because continuous crack propagation was observed in the DCB tests with these specimens, the mean values of the first half of the propagation were used. The open circles are the results from specimens 9 to 11 in Table 2. Because the crack propagated instantaneously after reaching the initial load peak with these specimens, the G_I values at this peak are used. In Fig. 10, pure mode I and pure mode II energy release rates are also plotted as open and closed squares, respectively. The G_I value for pure mode I was used for the plot obtained in a previous study (Sekiguchi et al., 2016) with the TDCB test following ASTM D3433-99 (2012). The G_{II} value for pure mode II was obtained with the ENF test.

The results indicate a negative correlation between the mode I and mode II energy release rates, which is in agreement with previous studies that used different test methods (Chaves et l., 2011, 2014a, 2014b; da Silva et al., 2012; Reeder and Crews Jr., 1990; Singh et al., 2010). In addition, mixed mode fractures were observed with continuous crack propagation over a wide range of the mode angles (maximum at 81.4 degrees). The linear energy criterion

$$\frac{G_{\mathrm{I}}}{G_{\mathrm{I,pure}}} + \frac{G_{\mathrm{II}}}{G_{\mathrm{II,pure}}} = 1 \tag{19}$$

is plotted as dashed dotted line in Fig. 10, where the mode I and mode II energy release rates are normalized by pure mode values, $G_{\mathrm{I,pure}}$ and $G_{\mathrm{II,pure}}$, respectively. It is sufficiently confirmed that the sum of the normalized mode I and mode II energy release rates is almost constant.

5 Conclusions

Double cantilever beam test specimens with residual stresses (DCB-rs) were manufactured and fracture tests were conducted. Because shear loads were generated at the adhesive layer in the manufacturing process, opening loads caused mixed mode fractures of the DCB-rs specimens with constant mixed mode ratios during each test. The mode I and mode II energy release rates were measured independently. A four point bending jig was used to manufacture the DCB-rs specimens, and the magnitude of the applied residual stresses was changed by the indentation depth of the jig. It was revealed that the residual stress that arises at the adhesive layer can be increased to generate pure mode II fractures. Additionally, the DCB test results indicated that the mode I energy release rate decreased with the increasing curvature of the manufactured DCB-rs specimens. The mode II energy release rate was theoretically obtained as a function of the radius of the curvature of the specimen. Then, it was estimated for each manufactured specimen by measuring the radius. By comparing the mode I and mode II energy release rates, a negative correlation was found, similarly to many other mixed mode fracture tests. Although unstable crack propagations were observed with mixed mode angles over approximately 80 degrees, the experiments indicated that DCB tests with DCB-rs specimens can cover

a wide range of the mixed mode ratios.

Acknowledgements

This study was conducted as a part of the Japanese METI project “The Future Pioneering Projects/Innovative Structural Materials Project”, which has been in progress since 2013. In addition, this paper is based on the results obtained from a future pioneering program commissioned by the New Energy and Industrial Technology Development Organization (NEDO).

References

ASTM D3433-99, 2012. Standard test method for fracture strength in cleavage of adhesives in bonded metal joints. ASTM International, West Conshohocken, PA.

ASTM D5528-01, 2007. Standard test method for mode I interlaminar frcavture toughness of unidirectional fiber-reinforced polymer matrix composites. ASTM International, West Conshohocken, PA.

ASTM D6671-06, 2006. Standard test method for mixed mode I-mode II interlaminar fracture toughness of unidirectional fiber reinforce polymer matrix composites. ASTM International, West Conshohocken, PA.

ASTM D7905-14, 2014. Standard test method for determination of the mode II interlaminar fracture toughness of unidirectional fiber-reinforced polymer matrix composites. ASTM International, West Conshohocken, PA.

Banea, M.D., da Silva, L.F.M, Camphilho, R.D.S.G., 2012. Mode II fracture toughness of adhesively bonded joints as a function of temperature: experimental and numerical study. J. Adhes. 88, 534-551. DOI: 10.1080/00218464.2012.660835

Blackman, B.R.K., Linloch, A.J., Paraschi, M., Teo, W.S., 2003. Measuring the mode I adhesive fracture energy, GIC, of structural adhesive joints: the results of an international round-robin, Int. J. Adhes. Adhes. 23, 293-305. DOI: 10.1016/S0143-7496(03)00047-2

Blackman, B.R.K., Kinloch, A.J., Paraschi, M., 2005. The determination of the mode II adhesive fracture resistance, GIIC, of structural adhesive joints: an effective crack length approach, Eng. Fract. Mech. 72, 877-897. DOI: 10.1016/j.engfracmech.2004.08.007

Chaves, F.J.P., de Moura, M.F.S.F., da Silva, L.F.M., Dillard, D.A., 2011. Numerical analysis of the dual actuator load test applied to fracture characterization of bonded joints, Int. J. Solids Struct. 48, 1572-1578. DOI: 10.1016/j.ijsolstr.2011.02.006

Chaves, F.J.P., da Silva, L.F.M., de Moura, M.F.S.F., Dillard, D.A., Esteves, V.H.C., 2014. Fracture mechanics tests in adhesively bonded joints: A literature review, J. Adhes. 90, 955-992. DOI: 10.1080/00218464.2013.859075

Chaves, F.J.P., de Moura, M.F.S.F., da Silva, L.F.M., Dillard, D.A., 2014. Fracture characterization of bonded joints using the dual actuator load apparatus, J. Adhes. Sci. Technol. 28, 512-524. DOI: 10.1080/01694243.2013.845357

da Silva, L.F.M., de Magalhães, Chaves, F.J.P., de Moura, M.F.S.F., 2010. Mode II fracture toughness of a brittle and a ductile adhesive as a function of the adhesive thickness, J. Adhes. 86, 891-905. DOI: 10.1080/00218464.2010.506155

da Silva, L.F.M., Dillard, D.A., Blackman, B., Adams, R.D., 2012. Testing adhesive joints: Best practices. Wiley-VCH Verlag & Co., Weinheim.

Davidson, B.D., Sundararaman, V., 1996. A single leg bending test for interfacial fracture toughness determination, Int. J. Fract. 78, 193-210. DOI: 10.1007/BF00034525

Davies, P., Sims, G.D., Blackman, B.R.K., Brunner, A.J., Kageyama, K., Hojo, M., Tanaka, K., Murri, G., Rousseau, C., Gieseke, B., Martin, R.H., 1999. Comparison of test configurations for determination of mode II interlaminar fracture toughness results from international collaborative test programme, Plastics, Rubber and Compos. 28, 432-437. DOI: 10.1179/146580199101540600

de Moura, M.F.S.F., Campilho, R.D.S.G., Gonçalves, J.P.M., 2009. Pure mode II fracture characterization of composite bended joints, Int. J. Solids Struct. 46, 1589-1595. DOI:

10.1016/j.ijsolstr.2008.12.001

Dillard, D.A., Singh, H.K., Park, S., Ohanehi, D., McGaw, M.A., 2006. A dual-actuator load frame for mixed-mode fracture of laminated or adhesively bonded specimens, Proceedings of the 2006 SEM Annual Conference and Exposition on Experimental and Applied Mechanics, 22973 (10pages).

Fernlund, G., Spelt, J.K., 1994. Mixed-mode fracture characterization of adhesive joints, Compos. Sci. Technol. 50, 441-449. DOI: 10.1016/0266-3538(94)90052-3

Franco, A., Royer-Carfagni, G., 2016. Contact stresses in adhesive joints due to different thermal expansion with the adherends, Int. J. Solids Struct. 87, 26-38. DOI: 10.1016/j.ijsolstr.2016.02.036

Galuppi, L., Royer-Carfagni, G., 2015. Localized contacts, stress concentrations and transient states in bent-lamination with viscoelastic adhesion. An analytical study, Int. J. Mech. Sci. 103, 275-287. DOI: 10.1016/j.ijmecsci.2015.08.016

Galuppi, L., Royer-Carfagni, G., 2015. Optimal cold bending of laminated glass, Int. J. Solids Struct. 67-68, 231-243. DOI: 10.1016/j.ijsolstr.2015.04.023

Galuppi, L., Royer-Carfagni, G., 2015. Cold-lamination-bending of glass: Sinusoidal is better than circular, Compos. Part B. 79, 285-300. DOI: 10.1016/j.compositesb.2015.04.024

ISO 15024, 2001. Fiber-reinforced plastic composites – Determination of mode I interlaminar fracture toughness, GIC, for unidirectionally reinforced materials. International Organization for Standardization, Geneva.

Martin, R.H., Davidson, B.D., 1999. Mode II fracture toughness evaluation using four point bend, end notched flexure test, Plastics, Rubber and Compos. 28, 401-406. DOI: 10.1179/146580199101540565

Nairn, J.A., 2000. Energy release rate analysis for adhesive and laminate double cantilever beam specimens emphasizing the effect of residual stresses, Int. J. Adhes. Adhes. 20, 59-70. DOI: 10.1016/S0143-7496(99)00016-0

Oliveira, J.M.Q., de Moura, M.F.S.F., Silva, M.A.L., Morais, J.J.L., 2007. Numerical analysis of the

MMB test for mixed-mode I/II wood fracture, Compos. Sci. Technol. 67, 1764-1771. DOI: 10.1016/j.compscitech.2006.11.007

Park, S., Dillard, D.A., 2007. Development of a simple mixed-mode fracture test and the resulting fracture energy envelope for an adhesive bond, Int. J. Fract. 148, 261-271. DOI: 10.1007/s10704-008-9200-z

Reeder, J.R., Crews Jr., J.R., 1990. Mixed-mode bending method for delamination testing, AIAA J. 28:7, 1270-1276. DOI: 10.2514/3.25204

Schuecker, C., Davidson, B.D., 2000. Evaluation of the accuracy of the four-point bend end-notched flexure test for mode II delamination toughness determination, Compos. Sci. Technol. 60, 2137-2146. DOI: 10.1016/S0266-3538(00)00113-5

Sekiguchi, Y., Katano, M., Sato, C., 2016. Experimental study of the mode I adhesive fracture energy in DCB specimens bonded with a polyurethane adhesive, J. Adhes. in press. DOI: 10.1080/00218464.2015.1070101

Shimamoto, K., Sekiguchi, Y., Sato, C., 2016. The critical energy release rate of welded joints between fiber-reinforced thermoplastics and metals when thermal residual stress is considered, J. Adhes. 92, 306-318. DOI: 10.1080/00218464.2015.1031339

Singh, H.K., Chakraborty, A., Frazier, C.E., Dillard, D.A., 2010. Mixed mode fracture testing of adhesively bonded wood specimens using a dual actuator load frame, Holzforshung, 64, 353-361. DOI: 10.1515/HF.2010.041

Timoshenko, S., 1925. Analysis of bi-metal thermostats, J. Opt. Soc. Am. 11, 233-255. DOI: 10.1364/JOSA.11.000233

Xiao, F., Hui, C.Y., Kramer, E.J., 1993. Analysis of a mixed mode fracture specimen: the asymmetric double cantilever beam, J. Mater. Sci. 28, 5620-5629. DOI: 10.1007/BF00367838

Yoon, S.H., Hong, C.S., 1990. Modified end notched flexure specimen for mixed mode interlaminar fracture in laminated composites, Int. J. Fract. 43, R3-R9. DOI: 10.1007/BF00018129

Table 1. Properties of the adherend.

Material	Young's modulus [GPa]	Yield strength [GPa]	Tensile strength [GPa]	Thickness [mm]
SUP 10	206	1.08	1.23	2

Table 2. Results of the indentation depth, radius of specimen curvature, and mode II energy release rate for each specimen.

No.	Indentation depth d [mm]	Back-calculated indentation depth d [mm]	Radius of specimen curvature ρ [mm]	Mode II energy release rate G_{II} [J/m^2]
1	0.2	0.65	2980	21.7
2	1.0	1.46	1330	109
3	2.2	2.42	804	297
4	3.0	3.24	601	532
5	3.0	3.24	600	534
6	4.0	4.16	467	882
7	4.0	4.30	452	941
8	4.6	4.85	401	1196
9	4.6	4.94	394	1240
10	5.0	5.09	382	1320
11	5.0	5.27	369	1410
12	6.0	N/A	N/A	N/A

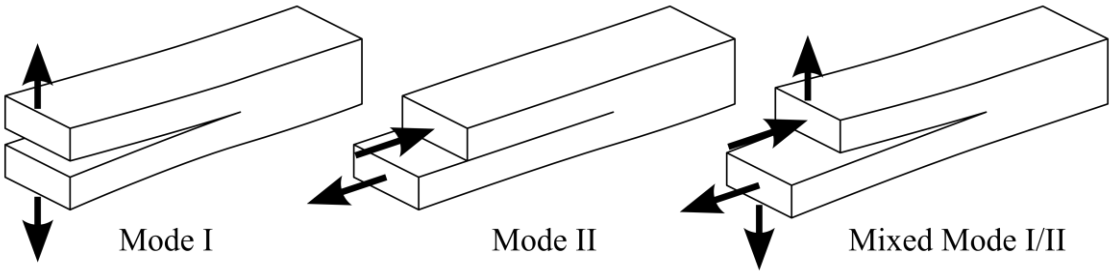

Figure 1 Schematic illustration of Mode I, Mode II, and Mixed Mode I/II.

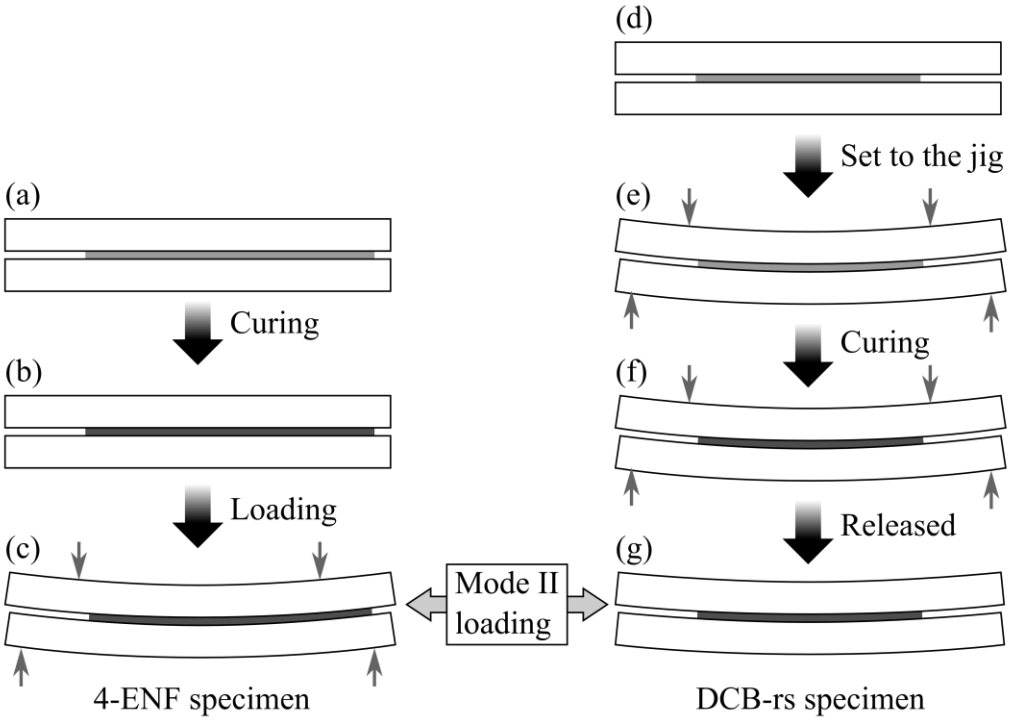

Figure 2. Schematic illustration of (a)-(c) the four point end notched flexure test and (d)-(g) DCB-rs specimen manufacturing.

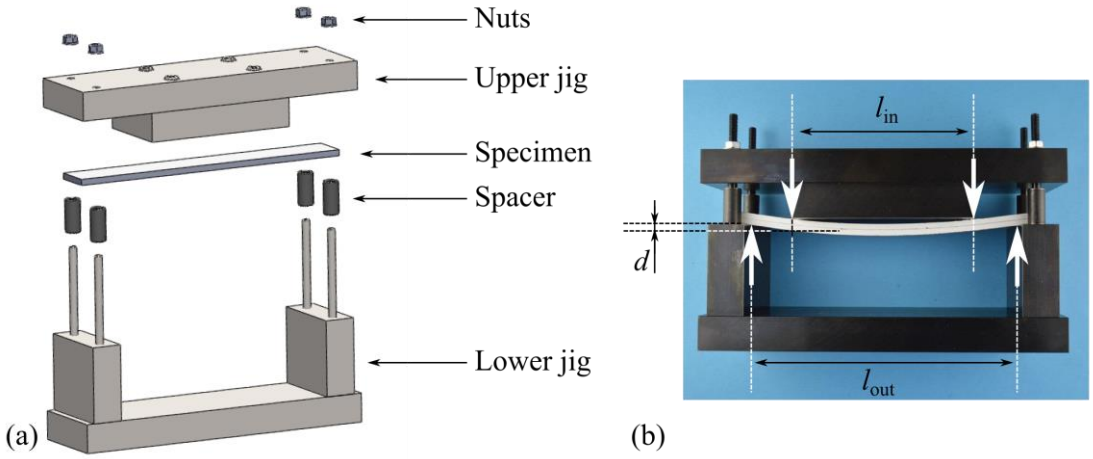

Figure 3. Four point bending jig (a) schematic illustration with each part separated, (b) side view of the jig when the specimen is set.

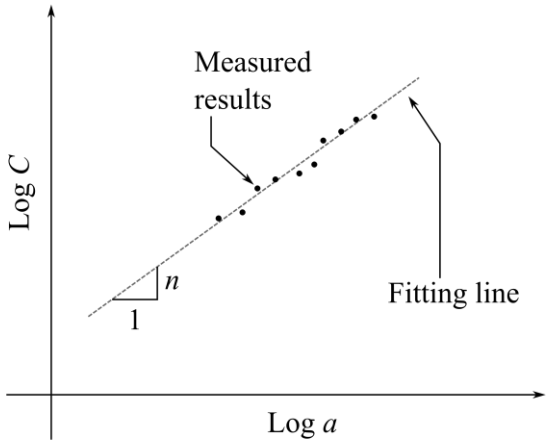

Figure 4. Schematic illustration of Log C versus Log a relation to obtain a constant n.

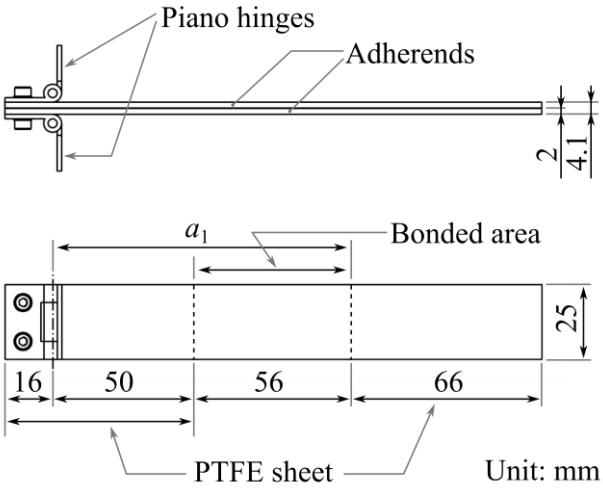

Figure 5. Configuration and dimensions of the DCB-rs specimen.

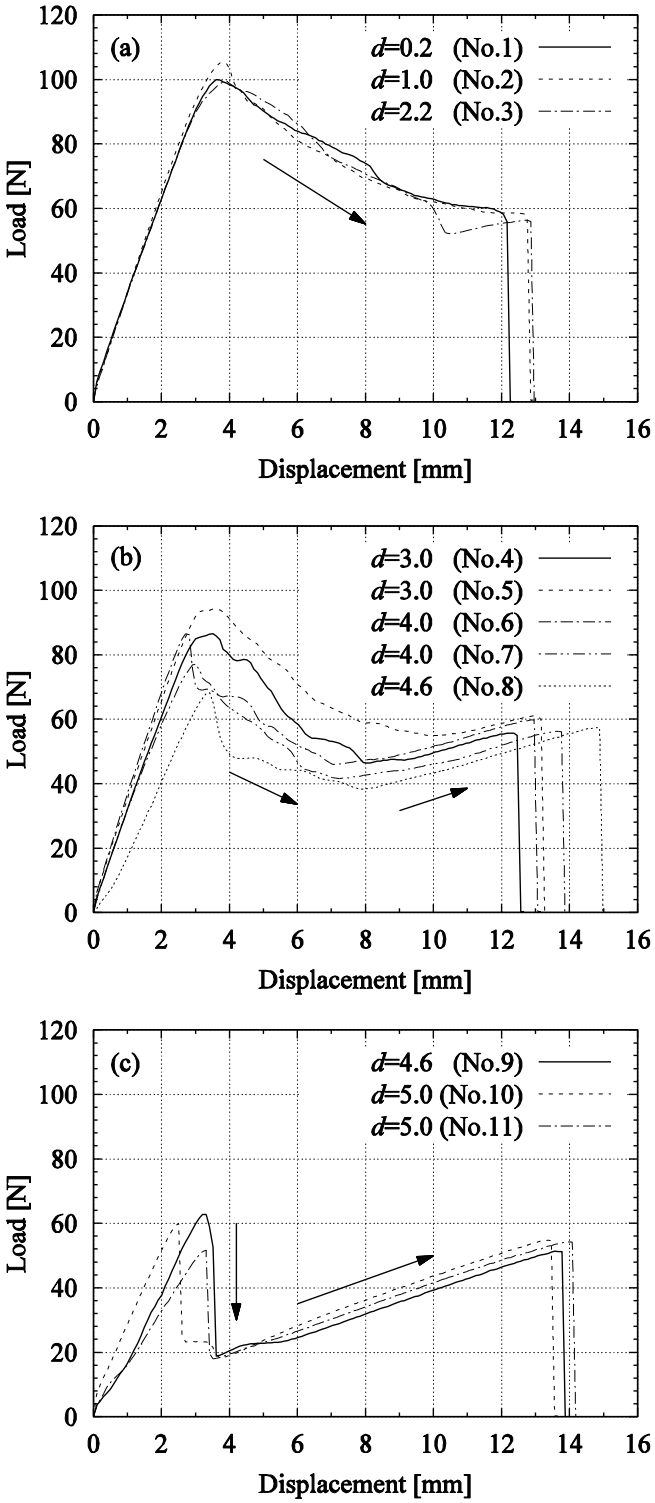

Figure 6. Load-displacement diagrams of the DCB tests with the DCB-rs specimens

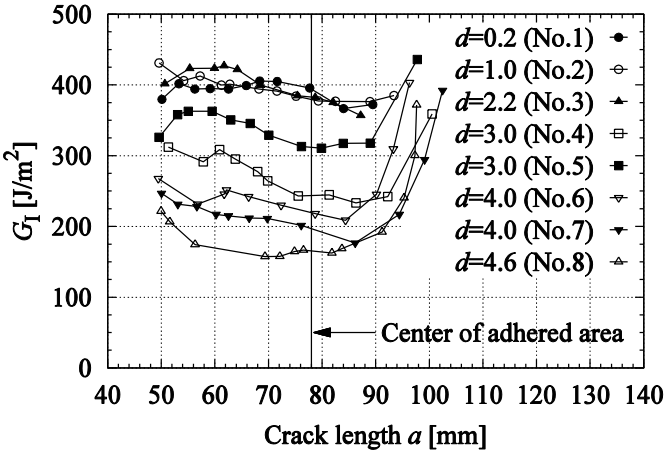

Figure 7. Mode I energy release rates of the DCB tests with the DCB-rs specimens

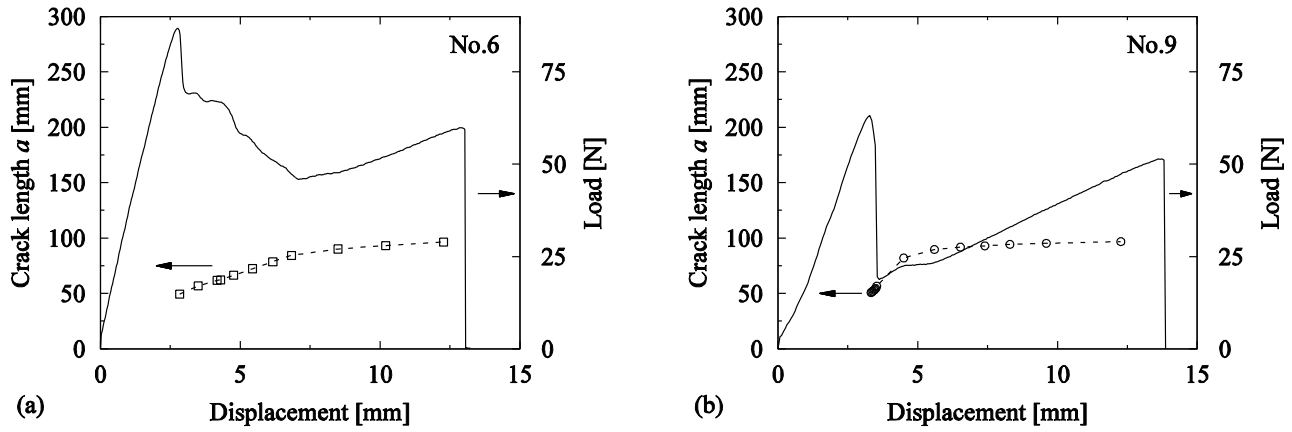

Figure 8. Crack length and load against displacement in the case of (a) No.6 and (b) No.9.

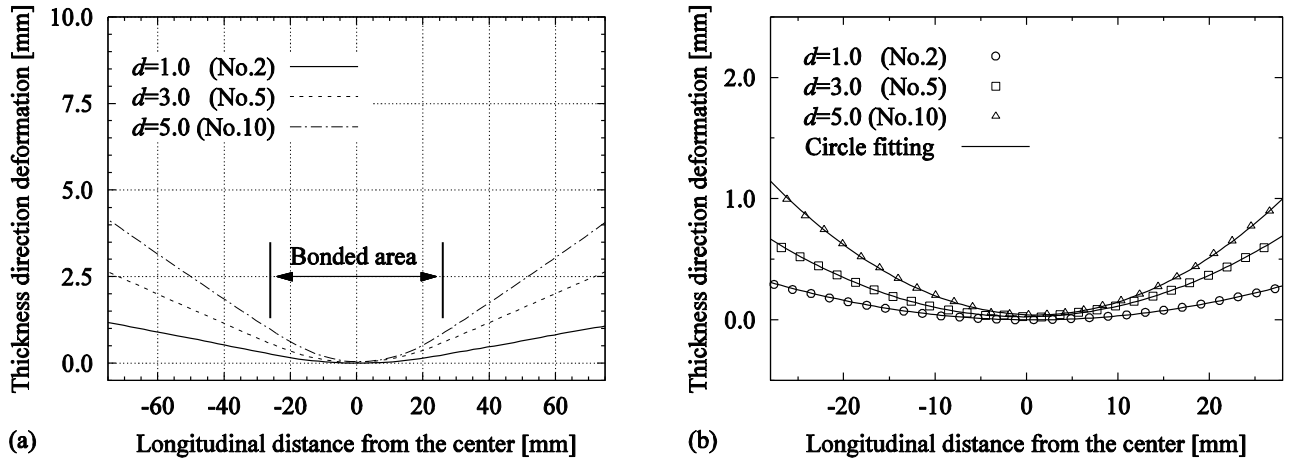

Figure 9. (a) Deformation of the DCB-rs specimens, and (b) enlarged view of the bonded area with

circle fitting curves.

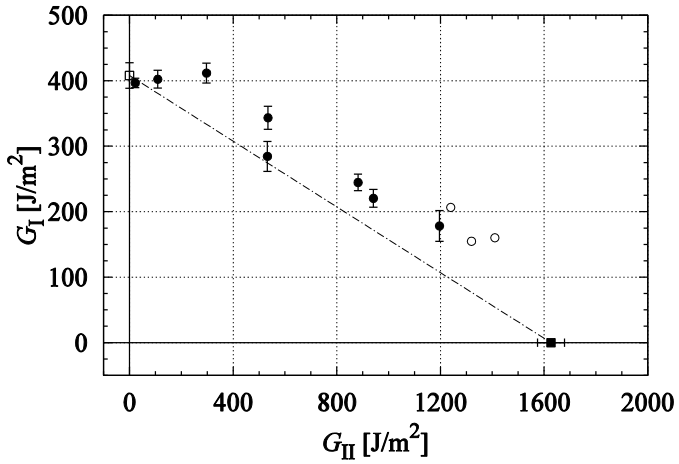

Figure 10. Mixed mode I/II energy release rate with the DCB-rs specimens.